

Podiform chromitites in the lherzolite-dominant mantle section of the Isabela ophiolite, the Philippines

メタデータ	言語: eng 出版者: 公開日: 2017-10-03 キーワード (Ja): キーワード (En): 作成者: メールアドレス: 所属:
URL	https://doi.org/10.24517/00010798

This work is licensed under a Creative Commons Attribution-NonCommercial-ShareAlike 3.0 International License.



Thematic Article

Podiform chromitites in the lherzolite-dominant mantle section of the Isabela ophiolite, the Philippines

TOMOAKI MORISHITA,^{1,*} ERIC S. ANDAL,¹ SHOJI ARAI¹ AND YOSHITO ISHIDA²

¹Graduate School of Natural Science and Technology, Kanazawa University, Kanazawa 920-1192, Japan (email: moripta@kenroku.kanazawa-u.ac.jp) and ²Department of Earth Sciences, Faculty of Science, Kanazawa University, Kanazawa 920-1192, Japan

Abstract The Isabela ophiolite, the Philippines, is characterized by a lherzolite-dominant mantle section, which was probably formed beneath a slow-spreading mid-ocean ridge. Several podiform chromitites occur in the mantle section and grade into harzburgite to lherzolite. The chromitites show massive, nodular, layered and disseminated textures. Clinopyroxene (\pm orthopyroxene/amphibole) inclusions within chromian spinel (chromite hereafter) are commonly found in the massive-type chromitites. Large chromitites are found in relatively depleted harzburgite hosts having high-Cr# (Cr/(Cr + Al) atomic ratio = \sim 0.5) chromite. Light rare earth element (LREE) contents of clinopyroxenes in harzburgites near the chromitites are higher than those in lherzolite with low-Cr# chromite, whereas heavy REE (HREE) contents of clinopyroxenes are lower in harzburgite than in lherzolite. The harzburgite near the chromitites is not a residual peridotite after simple melt extraction from lherzolite but is formed by open-system melting (partial melting associated with influx of primitive basaltic melt of deeper origin). Clinopyroxene inclusions within chromite in chromitites exhibit convex-shaped REE patterns with low HREE and high LREE (+Sr) abundances compared to the host peridotites. The chromitites were formed from a hybridized melt enriched with Cr, Si and incompatible elements (Na, LREE, Sr and H₂O). The melt was produced by mixing of secondary melts after melt–rock interaction and the primitive basaltic melts in large melt conduits, probably coupled with a zone-refining effect. The Cr# of chromites in the chromitites ranges from 0.65 to 0.75 and is similar to those of arc-related magmas. The upper mantle section of the Isabela ophiolite was initially formed beneath a slow-spreading mid-ocean ridge, later introduced by arc-related magmatisms in response to a switch in tectonic setting during its obduction at a convergent margin.

Key words: melt–rock interaction, ophiolite, podiform chromitite, rare earth element, supra-subduction.

INTRODUCTION

Chromian spinel (chromite hereafter) is a ubiquitous accessory mineral in peridotites and is a primary chromium reservoir in the mantle. The chemical composition of chromite varies depend-

ing on the petrogenesis (crystallization from melt, residue after partial melting with variable degrees) and physical conditions (pressure, temperature, oxygen fugacity) of the host peridotites (e.g. Irvine 1965, 1967; Ozawa 1983; Dick & Bullen 1984; Arai 1992, 1994a,b). There are two types of chromite deposits (chromitite) – namely, stratiform and podiform chromitites. The stratiform chromitite lies within stratified igneous complexes, such as Bushveld, Muskox and Stillwater (e.g.

*Correspondence.

Received 2 June 2005; accepted for publication 28 October 2005.

Jackson 1969; Irvine 1977; Roach *et al.* 1998). In contrast, podiform chromitite typically occurs in ophiolites as lenticular- or pod-shaped bodies closely associated with dunite at the transition zone between layered gabbros and residual peridotites (e.g. Thayer 1964). The podiform chromitites sometimes cut the deformed and/or layered structure of the host peridotites (Cassard *et al.* 1981; Nicolas 1989).

Irvine (1975, 1977) proposed that mixing of Si-rich and primitive basaltic melts can crystallize chromite forming stratiform chromitites. This mechanism is generally attributed to the origin of the podiform chromitites (Arai & Yurimoto 1994; Zhou 1994). When primitive melts generated at the deeper part of the mantle move upward, they react with peridotite wall-rock to produce SiO₂-rich secondary melts by selective consumption of orthopyroxene, resulting in the formation of a dunite wall (Fisk 1986; Kelemen 1990).

Podiform chromitite is not, however, equally distributed among the ophiolites. Boudier and Nicolas (1985) divided ophiolites into two subtypes in terms of the peridotite sections: the lherzolite ophiolite type (LOT) and the harzburgite ophiolite type (HOT). Chromitite is generally common in the HOT but is almost absent or found in small, if any, amounts in the LOT (Boudier & Nicolas 1985; Noller & Carter 1986; Leblanc & Temagout 1989; Gervilla & Leblanc 1990; Nicolas & Al Azri 1991). Although cross-cutting dunite as a result of a melt-rock interaction is a well-documented process in the LOT, it is not always associated with chromitites (Quick 1981; Nicolas & Al Azri 1991). Arai and Abe (1995) and Arai (1997a,b) suggested that a moderately refractory harzburgite with chromite having an intermediate Cr# (~0.5) is the most suitable host for large-scale podiform chromitites, because the lherzolite wall is too low in Cr# to concentrate chromite. Arai and Abe (1995) investigated the natural products of the melt-mantle interaction between alkaline basalt melt and orthopyroxene in peridotite xenoliths ranging from harzburgite to lherzolite in compositions (Kawashimo, Japan). They found that chromite is concentrated only in reaction zones with harzburgite orthopyroxene, whereas no concentration of chromite is found in lherzolite orthopyroxene.

As the Philippine Islands is surrounded by complex plate boundaries, numerous ophiolites and ophiolitic rocks crop out (e.g. Yumul *et al.* 1997). The Isabela ophiolite is exposed along the eastern coast of the Luzon, and is among the least studied

ophiolite in the Philippines. Recently Andal *et al.* (2005) reported the general characteristics of the mantle section of the Isabela ophiolite as a lherzolite-dominant ophiolite between LOT and HOT. Although the Isabela ophiolite is a lherzolite-dominant ophiolite, several chromite mines have operated in the past. The present study presents the first general description and geochemical data on the chromitites and their host peridotites near the chromitites in the Isabela ophiolite. The origin of the Isabela chromitites is discussed in the context of the formation of chromitite in a lherzolite-dominant ophiolite.

GEOLOGICAL BACKGROUND

The Isabela ophiolite crops out along the eastern coast of northern Luzon extending for 90 km and lies along the eastern margin of the Philippine Mobile Belt (Fig. 1). The ophiolite shows a complete ophiolite sequence consisting of mantle peri-

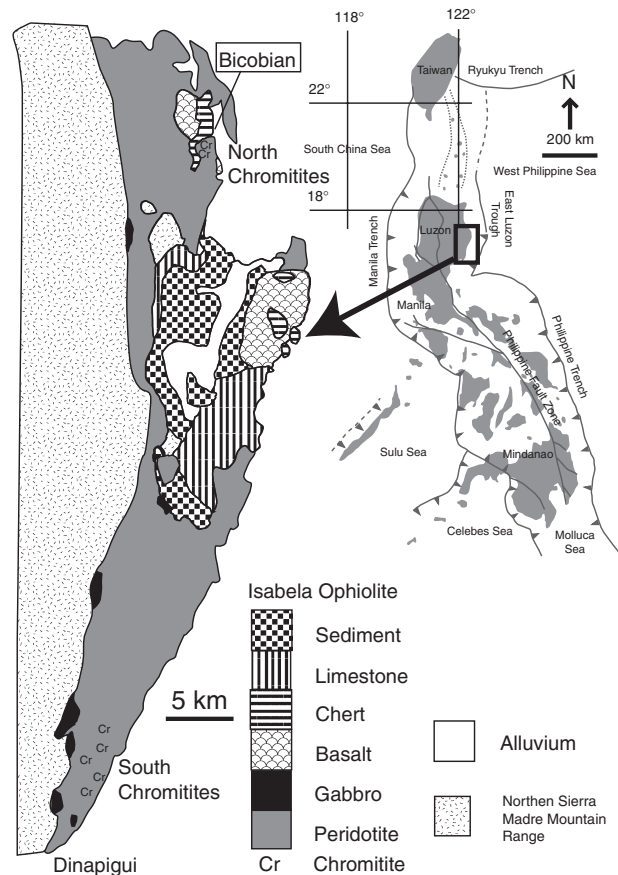


Fig. 1 Location of the chromite deposits on the lithological map around the Isabela ophiolite compiled by Andal *et al.* (2005). The tectonic map of the Philippine archipelago based on Dimalanta and Yumul (2004) and Andal *et al.* (2005) is also shown.

dotites, gabbros, basalts and cherts. The intrusive dyke complex, which is typical for the HOT, is not common (Billedo *et al.* 1996; Andal *et al.* 2005). These rocks are not sequentially distributed in the area (Fig. 1). Peridotites are mainly lherzolite to clinopyroxene-rich harzburgite with a granular to porphyroclastic texture and minor amounts of harzburgite, dunite and pyroxenite (Andal *et al.* 2005). Dunite occurs as thin layers or lenses ranging from a few centimeters to a few meters in thickness except for in the dunite envelopes around the chromitites as described below. They usually cut prominent mineral foliation of the host peridotites defined by pyroxene-rich and pyroxene-poor layers. Details of the peridotite structure are not clear yet, partly because of the extensive faulting and jointing along the entire length of the coastal exposure investigated in the present study. Chromite trails after pyroxenite are observed where a dunite layer cuts both peridotite and pyroxenites (Andal *et al.* 2005). Chromite is basically absent in thin dunite layers. A small chromite pod (10–15 cm in size) was found in a relatively thick dunite lens (~5 m wide) in the southern part (Andal *et al.* 2005). All peridotites are cut by gabbroic and/or clinopyroxenite veins. Several chromite mines have operated in both the northern (two mines) and the southern parts (five mines) of the studied area and have been abandoned (Fig. 1).

Andal *et al.* (2005) revealed general characteristics of peridotites in the studied area. Chromites in the residual peridotites from the whole studied area show a wide range of compositions (Fig. 2). Although samples from the southernmost part of the studied area (Dinapigui Point) contain chromites with very low Cr# (=Cr/(Cr + Al) atomic ratio) (0.08–0.16), the majority of the samples have chromite with 0.17–0.43 Cr#, correlating negatively with Mg# (Mg/(Mg + Fe²⁺) atomic ratio) (Fig. 2). The forsterite (Fo) content of olivine coexisting with chromite ranges from 88 to 92. Andal *et al.* (2005) also reported the constant decreasing of light rare earth element (LREE) from lherzolite to harzburgite far from the large chromitites (Fig. 3). These mineral compositions in clinopyroxene-bearing harzburgite and lherzolite are compatible with a residual origin and generally fall into the field of abyssal peridotites, particularly in slow-spreading ridges (Dick & Bullen 1984; Dick 1989; Johnson & Dick 1992; Arai 1994a,b) (Figs 3,4). The lherzolite-dominant mantle section, petrological discontinuities among the lithologies and the lack of a typical intrusive dyke complex

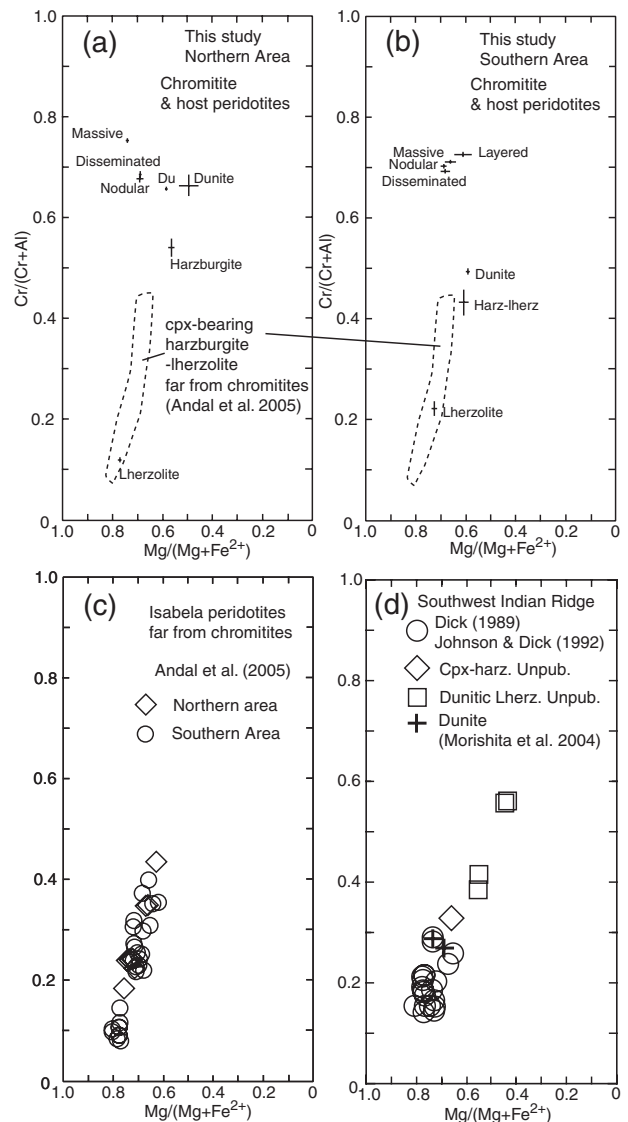


Fig. 2 Compositional relationship between Cr# (Cr/(Cr + Al) atomic ratio) and Mg# (Mg/(Mg + Fe²⁺) atomic ratio) of chromite. (a) Chromitites and their host peridotites near the chromitites in the northern area. Du, dunite layer alternating with chromite. (b) Chromitites and their host peridotites near the chromitites in the southern area. (c) Other peridotites far from chromitites in both the northern and the southern areas of the Isabela ophiolite. Data are from Andal *et al.* (2005). (d) Spinel peridotites from the Atlantis II Fracture Zone and Islas Orcadas Fracture Zone of the slow-spreading southwest Indian Ridge. These fracture zones are far from hot spots. (○), data from Dick (1989) and Johnson and Dick (1992). Data for dunite (+) with dunitic lherzolite (□) at the edge of the dunite-bearing sample and clinopyroxene-bearing harzburgite (◇) were collected from the eastern rift valley wall of the Atlantis II Fracture Zone during the ABCDE cruise using SHINKAI 6500 from the Japan Marine Science Technology Center (JAMSTEC) (Morishita *et al.* 2004; T. Morishita *et al.*, unpubl. data, 2005). It should be emphasized that (a), (b) and (c) do not represent frequency of rock types, because the samples were collected from the outcrop to cover a wide range of rock types during field work.

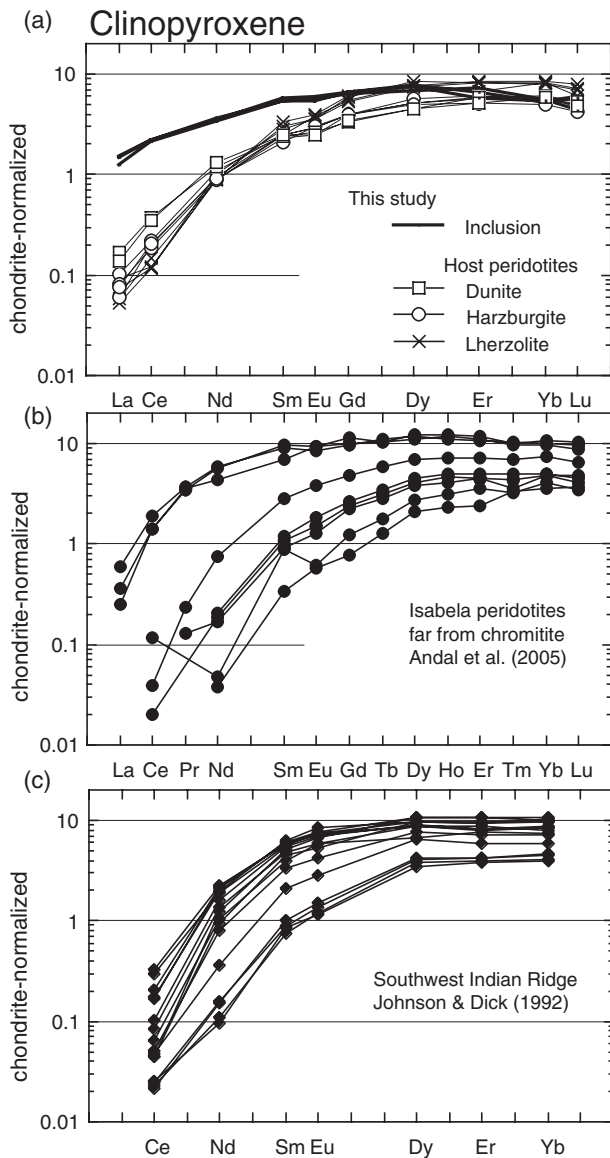


Fig. 3 Chondrite-normalized rare earth element patterns of clinopyroxenes. (a) Clinopyroxene inclusions within chromite, dunite-harzburgite-lherzolite near the chromitites. (b) Clinopyroxene from other peridotites far from the chromitites in the Isabela ophiolite. Data are from Andal *et al.* (2005). (c) Clinopyroxene from the Atlantis II Fracture Zone of the slow-spreading southwest Indian Ridge. Data are from Johnson and Dick (1992). Chondrite values are from McDonough and Sun (1995). Harz, harzburgite.

in the studied area support a slow-spreading ridge origin for the Isabela ophiolite (Andal *et al.* 2005). Based on the geochemical characteristics of peridotites, coupled with lithological variations, such as northward increasing of the degree of partial melting and increasing of dunite and gabbro veins, Andal *et al.* (2005) suggested that the northern part of the ophiolite represents the upper sections of the mantle column. Thus, the Isabela ophiolite may present a good analogy of the melting column

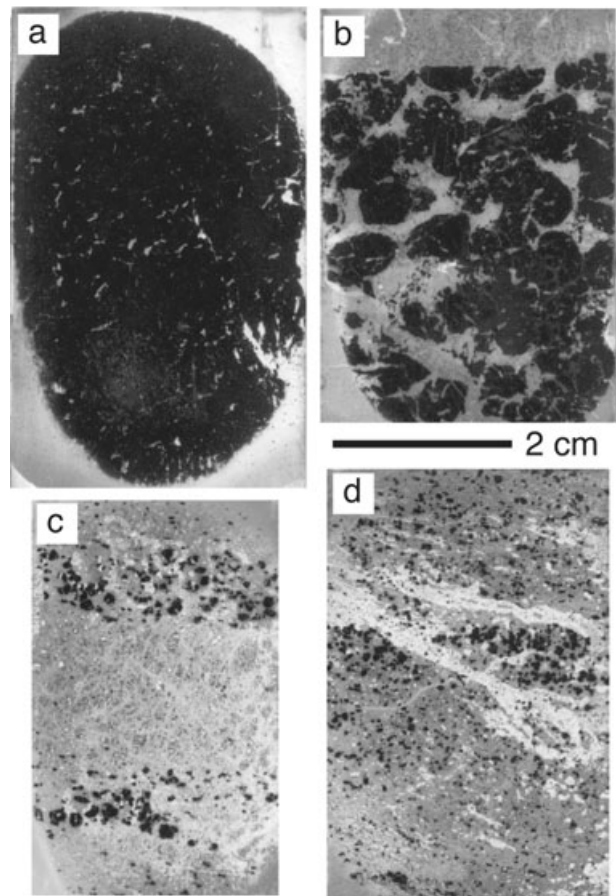


Fig. 4 Photographs showing textural variations of the chromitites. (a) Massive; (b) nodular; (c) layered; and (d) disseminated in the southern area. Textures of chromitites in the northern area are the same as those in the southern area.

beneath slow-spreading mid-ocean ridges (Andal *et al.* 2005).

SAMPLE DESCRIPTIONS

In the southern part, the main part of the chromitite bodies was almost mined out and the degree of serpentinization is relatively high in the peridotites around the chromitites. A few small chromitite blocks are still left along the wall rocks (dunite) in the southern chromitites. The northern chromite mines (Bicobian, Fig. 1) were not accessible in the present study. Instead, several samples, including both chromitites and peridotites, which may be from around the chromitites, were collected at the stockpile of these chromite mines at Port Bicobian (Fig. 1). Irrespective of limited outcrops and samples, all chromitites observed in the present study are always enclosed with dunite and can be estimated as having a pod-like shape not extending

Table 1 The numbers of primary silicate mineral inclusions within chromite in the chromitites

Sample name	Texture type	Ol	Cpx	Opx	Amph	Total
Southern chromitite						
2-1	Massive		4	1	1	6
2-2	Layer	13			1 [†]	14
2-3	Disseminated	18			1	19
2-5	Nodular	25			1	26
Northern chromitite						
5-7	Massive	1	5			6
5-6	Nodular	7	14	1		22
5-9	Disseminated	17				17

The numbers of the primary inclusions (olivine, clinopyroxene, orthopyroxene and amphibole) within chromitites in one thin section were counted for each sample except for 5-6 of the southern chromitites. The sample 5-6 has abundant inclusions within chromite. The numbers of inclusions were counted from less than half of the whole area of the thin section. It is noted that the data therefore do not represent the real frequency of primary inclusions. Some samples have no pyroxene inclusions although they have olivine inclusions, which are easily altered to serpentine and/or chlorite after reactions with water at low-temperature conditions. [†]Too small to identify the phase, which is high in Na and K.

amph, amphibole; cpx, clinopyroxene; ol, olivine; opx, orthopyroxene.

more than 300 m (chromitite + dunite envelope) in width. They are therefore typical podiform chromitites (e.g. Thayer 1964).

Massive, disseminated, nodular and layered chromitites are found in both the northern and the southern chromitites (Fig. 4). Weak flattening of the chromite nodules in nodular-type chromitite is found, and is nearly parallel to the lithological boundary between the dunitic layer and chromite-rich layer (Fig. 4b). The interstitial silicate matrix of the chromitites is olivine, now completely serpentized. It is noteworthy that harzburgites are always associated with the dunite envelope of the chromitites, although lherzolite is also found outward, meaning that the podiform chromitites have dunite envelopes grading outward into harzburgite to lherzolite.

Silicate mineral inclusions within chromites are commonly found in the chromitites. Low-temperature hydrous minerals (serpentine and chlorite) are formed where the inclusions are open to the surrounding minerals. Some of the primary silicate inclusions within the chromite still remain from alteration, and are olivine, clinopyroxene and amphibole/orthopyroxene in decreasing order of abundance (Table 1). Amphibole and orthopyroxene are rare. Phlogopite, which is commonly found as inclusions of chromites in many chromitites (e.g. Talkington *et al.* 1986; Augé 1987; Lorand & Ceuleneer 1989; McElduff & Stumpfl 1991; Schiano *et al.* 1997; Arai & Matsukage 1998), has not been found so far. Differences in resistance to low-temperature hydrous alteration during serpentization between olivine and pyroxenes result in the abundance of pyroxene inclusions in massive-type

chromitites (\pm nodular type) (Table 1). It is important to note that clinopyroxene, orthopyroxene and amphibole are not found as interstitial silicate minerals of the chromitites, although a dunite envelope of the chromitites sometimes contains minor clinopyroxene as anhedral grains between olivine grains.

MINERAL CHEMISTRY

ANALYTICAL METHODS

The major element compositions of minerals were analyzed with a JEOL JXA-8800 Superprobe at the Center for Cooperative Research of Kanazawa University. The analyses were performed with an accelerating voltage of 15–20 kV and a beam current of 15–20 nA using a 3- μ m-diameter beam. JEOL software using ZAF corrections was used. Trace element compositions (Li, Sc, Ti, V, Cr, Rb, Sr, Y, Zr, Nb, Ba, REE, Hf and Pb) of clinopyroxenes (inclusions of chromites [>50 μ m in size] in chromitites and porphyroclast in peridotites) were analyzed by laser ablation (193 nm ArF excimer: MicroLas GeoLas Q-plus) inductively coupled plasma mass spectrometry (Agilent 7500S) (LA-ICP-MS) at the Incubation Business Laboratory Center of Kanazawa University (Ishida *et al.* 2004). Each analysis was performed by ablating 30- μ m and 50- μ m-diameter spots for inclusions and porphyroclasts, respectively, at 5 Hz. NIST SRM 612 glass was used as the primary calibration standard and was analyzed at the beginning of each batch of <6 unknowns, with a linear drift

correction applied between each calibration. The element concentration of NIST SRM 612 for the calibration was selected from the preferred values of Pearce *et al.* (1997). Data reduction was facilitated using ^{43}Ca as an internal standard element, based on CaO contents obtained by EPMA analysis, and followed a protocol essentially identical to that outlined by Longrich *et al.* (1996). Details of the analytical method and data quality for the LA-ICP-MS system at Kanazawa University are described in Morishita *et al.* (2005a,b). The representative analyses of both major and trace element compositions of minerals are shown in Tables 2 and 3, respectively.

MAJOR ELEMENT COMPOSITION OF MINERALS

Chromites

The Cr# of chromites from four chromite mines in the southern part and chromitite samples collected at a stockpile in the northern part shows only small variations, ranging from 0.65 to 0.75. Their Mg# decreases with increasing of mode of silicate minerals in the rock, probably as a result of subsolidus equilibrium at low-temperature conditions (e.g. Irvine 1965; Ozawa 1983). Samples collected from the northern part and the largest chromite mine (+surrounding host peridotites) in the southern part were examined in detail in the present study (Fig. 1). The chromite compositions in chromitites are slightly different, reflecting the differences in the textures: the massive (+layered) chromitites are more Cr-rich than the nodular and disseminated chromitites (Fig. 3). The Cr# of chromite in harzburgites and lherzolites near the chromitites shows a wide range of composition: 0.22 and 0.43 for the northern samples, and 0.12 and 0.54 for the southern samples. It is noted that the Cr# of chromite in the harzburgite near the chromitites fall into the high end or higher than whole range of those in harzburgite–lherzolite far from the chromitites (Fig. 2). Dunites with chromitites have chromite with relatively high Cr# and low Mg# (0.49 and 0.59 in the south, and 0.67 and 0.50 in the north). Some of these are similar to the lower range of those in the chromitite field (Fig. 2). The TiO_2 content of chromites increases from lherzolite (<0.09 wt%) to harzburgite (0.13–0.25 wt%) to dunite (<0.09–0.31 wt%) to chromitites (0.22–0.31 wt%) (Fig. 5). The $100\text{Fe}^{3+}\#$ ($100 \times \text{Fe}^{3+}/(\text{Cr} + \text{Al} + \text{Fe}^{3+})$ atomic ratio) of chromites tends to be higher in the dunite than others but is usually <0.1 (Table 2).

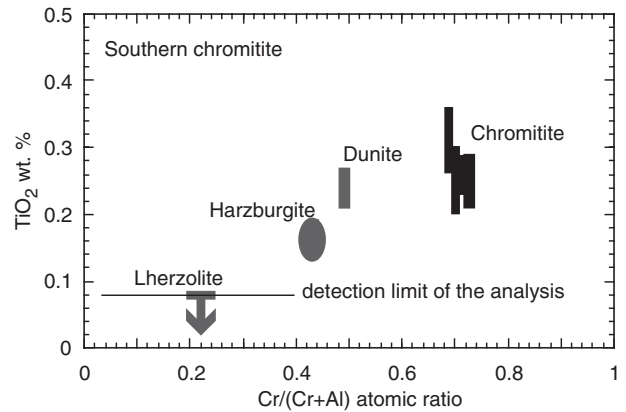


Fig. 5 Compositional relationship between Cr# ($\text{Cr}/(\text{Cr} + \text{Al})$ atomic ratio) and TiO_2 wt% of chromites in the chromitites and their host peridotites.

Silicate minerals in the host peridotites of the chromitites

The Fo and NiO contents of olivines are 90.5 and 0.4 wt% in lherzolite, 90.8 and 0.4 wt% in clinopyroxene-bearing harzburgite, and 90.9 and 0.4 wt% in dunite envelopes, respectively, for the southern chromitite (Table 2). The Al_2O_3 and Cr_2O_3 contents of the clinopyroxene core are 4.8 and 1.0 wt% in lherzolite (Cr# = 0.13), 2.9 wt% and 1.1 wt% in harzburgite (Cr# = 0.21), and 1.9–2.4 and 0.7–1.0 wt% (Cr# = 0.44–0.45) in dunite, respectively. The Al_2O_3 and Cr_2O_3 contents of the orthopyroxene core are 4.4 and 0.7 wt% in lherzolites (Cr# = 0.09), and 2.5 wt% and 0.7 wt% in harzburgites (Cr# = 0.15), respectively.

Silicate mineral inclusions within chromites in the chromitites

The Fo and NiO contents of olivine inclusions are 95–98 and 0.5–1.1 wt%, respectively (Table 2). These high Fo and NiO contents for olivine inclusions may result from subsolidus equilibration with the host chromites at lower-temperature conditions than their formations. Clinopyroxene inclusions have Mg# = 0.95–0.97, Al_2O_3 = 0.7–1.4 wt%, Cr_2O_3 = 1.0–1.8 wt%, TiO_2 ≤ 0.09–0.14 wt% and Na_2O = 0.3–0.4 wt%. Orthopyroxene inclusions have Mg# = 0.95, Al_2O_3 = 0.6–0.8 wt%, Cr_2O_3 = 0.7 wt% and TiO_2 ≤ 0.09 wt%. Amphibole inclusions within chromite in lherzolite are edenitic hornblende to pargasite in composition by the nomenclature of Leake *et al.* (1997). Their TiO_2 content (<1 wt%) is lower than those of independent pargasite grains in fertile lherzolites at Dinapigui Point (1.5–3.7 wt%, Andal *et al.* 2005).

Table 2 Major-element compositions of minerals in the chromitites and their host peridotites

Area: Rock type: Texture: Mineral: (Anal#):	North Chromitite Massive (5-7)						Nodular (5-6)				Disseminated (5-9)			
	Chr (n = 16)	STD (113)	Ol inc (113)	Cpx inc (119)	Chr (n = 6)	STD (n = 4)	Chr (d) (n = 4)	STD	Opx inc (32)	Chr (n = 17)	STD	Ol inc (n = 12)	STD	
(wt%):														
SiO ₂	<0.04	41.48	53.85	<0.04	<0.04	<0.04	0.03	57.29	<0.04	41.33	0.03	41.33	0.38	
TiO ₂	0.26	<0.09	<0.09	0.22	0.22	0.21	0.03	<0.09	0.22	<0.09	0.03	<0.09		
Al ₂ O ₃	12.82	0.14	0.93	16.82	16.82	17.43	0.34	0.82	15.92	<0.04	0.24	<0.04		
Cr ₂ O ₃	57.33	0.60	1.59	53.18	53.18	49.35	0.44	0.68	51.82	0.65	0.75	0.65	0.19	
FeO	13.20	0.29	1.27	14.50	14.50	19.04	0.43	3.24	14.89	3.06	0.35	3.06	0.21	
MnO	0.23	0.03	<0.07	0.24	0.24	0.32	0.03	0.08	0.23	<0.07	0.03	<0.07		
MgO	15.86	0.20	54.99	18.31	15.03	12.53	0.26	35.96	14.83	54.52	0.23	54.52	0.54	
CaO	<0.04	<0.04	22.62	<0.04	<0.04	<0.04	0.03	0.67	<0.04	<0.04	0.02	<0.04		
Na ₂ O	<0.04	<0.04	0.39	<0.04	<0.04	<0.04	0.28	<0.04	<0.04	<0.04	0.02	<0.04		
K ₂ O	<0.03	<0.03	0.05	0.13	0.12	0.07	0.03	<0.03	<0.03	<0.03	0.02	<0.03		
NiO	0.21	0.03	1.09	0.13	0.12	0.07	0.03	0.11	0.12	0.67	0.02	0.67	0.05	
total	99.96	0.74	100.46	99.29	100.16	98.99	0.52	98.85	98.10	100.36	0.63	100.36	0.90	
Numbers of ions on the basis of 4 oxygen ions for olivine and chromite, 6 oxygens for clinopyroxene and orthopyroxene, and 23 oxygen ions for amphibole														
O:	4	4	6	4	4	4	4	6	4	4	4	4	4	
Si	0.006	0.001	1.964	0.005	0.005	0.005	0.001	1.968	0.005	0.005	0.001	0.985	0.004	
Ti	0.479	0.006	0.040	0.619	0.619	0.659	0.011	0.033	0.601	0.009	0.009	0.012	0.003	
Al	1.437	0.009	0.010	1.314	1.314	1.252	0.006	0.037	1.312	0.016	0.016	0.061	0.004	
Cr	0.350	0.007	0.044	0.379	0.379	0.511	0.011	0.043	0.399	0.010	0.010	0.061	0.004	
Fe	0.006	0.001	0.001	0.006	0.006	0.009	0.001	0.002	0.006	0.001	0.001	0.009	0.007	
Mg	0.750	0.009	1.946	0.995	0.700	0.599	0.013	1.847	0.708	1.847	0.009	1.935	0.007	
Ca			0.884	0.028	0.028	0.020	0.025	0.025	0.025	0.025	0.000	0.000		
Na			0.002	0.002	0.002	0.002	0.000	0.000	0.000	0.000	0.000	0.000		
K			0.004	0.004	0.003	0.001	0.001	0.003	0.003	0.001	0.001	0.013	0.001	
Ni	3.034	0.003	3.007	3.027	3.027	3.037	0.002	3.996	3.036	0.004	0.004	3.006	0.003	
total	0.740	0.009	0.978	0.962	0.692	0.591	0.013	0.958	0.698	0.008	0.008	0.969	0.002	
Mg#	0.750	0.003	0.535	0.680	0.680	0.655	0.006	0.479	0.656	0.006	0.006	0.006		
Cr#	4.3	0.3	3.4	3.4	3.4	4.8	0.3	4.6	4.6	0.6	0.6	4.6		
Y Fe	23.9	0.3	31.0	31.0	31.0	32.8	0.6	30.0	30.0	0.4	0.4	30.0		
Y Al	71.8	0.5	65.6	65.6	65.6	62.4	0.5	65.4	65.4	0.9	0.9	65.4		
Y Cr														

Table 2 Continued

Dumite			Harzburgite			Lherzolitite			Massive (2-1) Chr (n = 16)			South Chromitite			Amph (51)
Chr (n = 16)	STD	Chr (n = 16)	STD	Cpx (56)	Chr (n = 12)	STD	Chr (n = 16)	STD	Chr (n = 16)	STD	Cpx inc (55)	Cpx inc (71)	Cpx inc (73)	Opx inc (64)	
<0.04		<0.04		53.74	<0.04		<0.04		<0.04		53.42	53.74	54.25	58.31	46.50
0.16	0.05	<0.09		0.09	<0.09		<0.09		0.26		0.14	0.16	<0.09	<0.09	0.93
15.25	0.98	23.45	0.91	2.20	56.58	0.59	14.98		14.98		1.13	0.97	1.12	0.61	9.03
45.77	1.04	41.27	1.55	0.91	11.13	0.46	54.71		54.71		1.31	1.35	1.30	0.74	3.30
26.34	1.31	22.21	0.54	1.89	11.68	0.37	15.98		15.98		1.57	1.54	1.46	3.29	1.79
0.35	0.03	0.31	0.03	0.06	0.12	0.03	0.27		0.27		<0.07	<0.07	0.08	0.08	0.06
10.17	0.85	12.35	0.25	17.07	19.83	0.22	14.17		14.17		18.12	18.30	18.09	37.67	20.34
<0.04		<0.04		24.14	<0.04		<0.04		<0.04		22.14	22.22	22.25	0.45	11.21
<0.04		<0.04		0.17	<0.04		<0.04		<0.04		0.43	0.39	0.42	<0.04	2.86
<0.03		<0.03		0.04	<0.03		<0.03		<0.03		<0.03	<0.03	<0.03	0.04	<0.03
0.13	0.02	0.11	0.03	0.04	0.36	0.02	0.13		0.13		<0.07	<0.07	<0.07	0.14	0.18
98.22	0.54	99.84	0.74	100.30	99.79	0.76	100.55		100.55		98.37	98.82	99.10	101.33	96.23
4		4		6	4		4		4		6	6	6	6	23
				1.946							1.965	1.968	1.977	1.964	6.641
0.004	0.001	0.864	0.032	0.002	1.743	0.009	0.006		0.006		0.004	0.004	0.048	0.024	0.099
0.604	0.034	0.094	0.038	0.094	0.230	0.010	0.558		0.558		0.049	0.042	0.048	0.020	1.519
1.215	0.032	1.020	0.016	0.026	0.255	0.008	1.366		1.366		0.038	0.039	0.037	0.020	0.372
0.740	0.044	0.581	0.001	0.057	0.003	0.001	0.422		0.422		0.048	0.047	0.044	0.093	0.214
0.010	0.001	0.008	0.010	0.002	0.772	0.005	0.007		0.007		0.002	0.002	0.002	0.002	0.008
0.509	0.038	0.576	0.010	0.921	0.003	0.005	0.667		0.667		0.993	0.998	0.982	1.890	4.327
				0.936							0.872	0.871	0.868	0.016	1.714
				0.012							0.031	0.028	0.030	0.002	0.791
0.003	0.001	0.003	0.001	0.001	0.008	0.001	0.003		0.003					0.004	0.005
3.085	0.005	3.052	0.005	3.998	3.010	0.003	3.030		3.030		4.000	3.997	3.990	4.015	0.020
0.495	0.037	0.566	0.010	0.941	0.771	0.005	0.659		0.659		0.954	0.955	0.957	0.953	15.712
0.668	0.018	0.541	0.018	0.216	0.117	0.005	0.710		0.710		0.436	0.483	0.438	0.450	0.953
10.8	0.6				1.3	0.4	3.8		3.8						0.197
29.6	1.7				87.2	0.4	27.9		27.9						
59.6	1.6				11.5	0.5	68.3		68.3						

Table 2 *Continued*

Nodular (2-5)		Disseminated (2-13)			Layered (2-2)							
Chl (n = 11)	STD	Ol inc (n = 11)	STD	Amph (25)	Chr (n = 19)	STD	Amph (35)	Chr (n = 15)	STD	Ol (n = 10)	Layered (2-2)	Ol inc (n = 13)
<0.04		41.63	0.19	44.46	<0.04	0.01	43.11	<0.04	0.38	41.13	0.13	41.25
0.25	0.05	<0.09		0.96	0.31	0.05	0.54	0.25		<0.09		<0.09
15.02	0.26	<0.04		11.09	15.69	0.15	12.27	13.66		<0.04		<0.04
52.86	0.76	<0.1	0.24	3.08	53.10	0.75	3.13	54.25	0.26	<0.1		0.40
15.35	0.30	3.19	0.22	1.92	15.81	0.68	2.12	18.06	0.28	6.36	0.19	4.50
0.24	0.03	<0.07		0.09	0.25	0.03	<0.07	0.29		0.09	0.02	0.08
14.73	0.25	54.24	0.40	19.18	14.79	0.44	18.92	12.88	0.62	51.87	0.44	53.37
<0.04		<0.04		12.17	<0.04	0.01	13.24	<0.04		0.10	0.02	0.09
<0.04		<0.04		3.18	<0.04	0.01	3.34	<0.04		<0.04		<0.04
<0.03		<0.03		0.24	<0.03	0.01	0.39	<0.03		<0.03		<0.03
0.12	0.02	0.66	0.05	0.12	0.12	0.03	0.15	0.10	0.05	0.44	0.03	0.51
98.60	0.72	100.36	0.61	96.49	100.12	0.76	97.23	99.57	0.77	100.05	0.58	100.24
4		4		23	4	n = 19	23	4		4		4
0.006	0.001	0.991	0.003	6.382	0.007	0.001	6.190	0.006	0.004	0.994	0.004	0.989
0.568	0.009			0.103	0.584	0.006	0.058	0.521				
1.340	0.014			1.876	1.324	0.010	2.075	0.355				
0.412	0.010	0.064	0.005	0.350	0.417	0.020	0.254	1.388	0.005	0.129	0.004	0.008
0.006	0.001	0.001	0.000	0.230	0.007	0.001	0.003	0.489	0.006	0.002	0.000	0.090
0.704	0.010	1.924	0.006	0.011	0.695	0.018	4.046	0.008	0.010	1.868	0.007	1.906
				4.102	0.007	0.018	2.037	0.621		0.003	0.000	0.002
				1.871	0.695	0.018	2.037	0.621		0.003	0.000	0.002
				0.885	0.007	0.018	0.928	0.621		0.003	0.000	0.002
				0.044	0.003	0.001	0.071	0.003		0.009	0.001	0.010
0.003	0.001	0.013	0.001	0.014	0.003	0.001	0.017	0.003	0.001	0.009	0.001	0.010
3.039	0.004	2.992	0.003	15.867	3.037	0.004	16.036	3.037	0.004	3.004	0.004	3.006
0.693	0.010	0.968	0.002	0.947	0.684	0.018	0.941	0.612	0.003	0.936	0.002	0.955
0.702	0.005			0.157	0.694	0.004	0.146	0.727	0.006	0.006	0.006	0.984
5.0	0.6			4.8	4.8	0.5	4.8	4.8	0.4	0.4	0.4	
28.3	0.4			29.1	29.1	0.3	26.0	26.0	0.6	0.6	0.6	
66.8	0.8			66.1	66.1	0.6	69.2	69.2	0.8	0.8	0.8	

Table 2 Continued

Dumite		Harzburgite										Lherzolitite							
Ol (n = 6)	STD	Cpx (46)	Cpx (56)	Cpx (62)	Chr (n = 7)	STD	Ol (n = 7)	STD	Opx c (83)	Cpx (100)	Chr (n = 13)	STD	on inc (79)	Ol (n = 7)	STD	Opx c (32)	Cpx c (24)	Chr (n = 9)	STD
40.76	0.18	53.57	53.12	53.69	<0.04	0.17	41.57	0.17	57.49	53.53	<0.04	0.03	41.81	40.67	0.32	55.30	51.61	<0.04	
<0.09		0.20	0.24	0.19	0.24	0.03	<0.09		0.12	0.14	0.16	0.03	<0.09	<0.09		<0.09	0.29	<0.09	
<0.04		2.27	2.42	1.88	27.09	0.50	<0.04		2.52	2.85	31.31	1.71	<0.04	<0.04		4.44	4.75	47.26	1.32
<0.1		0.96	0.98	0.73	39.16	0.56	<0.1		0.68	1.12	35.50	1.91	0.77	<0.1	0.08	0.65	1.08	19.95	1.23
8.90	0.19	2.24	2.13	1.90	19.58	0.38	8.94	0.11	5.82	2.17	18.27	0.97	7.05	9.29	0.33	6.45	2.45	13.86	0.56
0.12	0.03	0.07	0.15	<0.07	0.24	0.03	0.12	0.03	0.14	0.05	0.24	0.03	0.13	0.14	0.04	0.18	<0.07	0.16	0.02
50.10	0.20	17.21	17.12	17.05	13.20	0.23	49.74	0.28	34.12	16.96	13.83	0.44	51.45	49.71	0.49	33.72	16.71	17.81	0.31
<0.04		22.91	22.64	23.18	<0.04		<0.04		0.64	23.89	<0.04		<0.04	<0.04	0.02	0.55	24.19	<0.04	
<0.04		0.47	0.46	0.37	<0.04		<0.04		<0.04	0.38	<0.04		<0.04	<0.04		<0.04	0.25	<0.04	
<0.03		<0.03	<0.03	<0.03	<0.03		<0.03		<0.03	<0.03	<0.03		<0.03	<0.03		<0.03	<0.03	<0.03	
0.36	0.03	<0.07	<0.07	<0.07	0.11	0.03	0.36	0.03	<0.07	<0.07	0.12	0.03	0.41	0.39	0.05	<0.07	<0.07	0.23	0.04
100.32	0.46	99.93	99.30	99.11	99.69	0.49	100.81	0.33	101.61	101.12	99.50	0.56	101.67	100.34	0.61	101.39	101.44	99.39	0.70
4		6	6	6	4		4		6	6	4		4	4		6	6	4	
0.994	0.003	1.946	1.941	1.963		0.003	1.007	0.003	1.949	1.926		0.001	0.998	0.994	0.004	1.889	1.860		
		0.005	0.007	0.005	0.006	0.001			0.003	0.004	0.004		0.000			0.008	0.008		
		0.097	0.104	0.081	0.974	0.015			0.101	0.121	1.102	0.051	0.000	0.001	0.002	0.179	0.202	1.528	0.033
0.181	0.004	0.028	0.028	0.021	0.945	0.014			0.018	0.032	0.838	0.051	0.014	0.001	0.002	0.018	0.031	0.433	0.029
0.003	0.001	0.068	0.065	0.058	0.500	0.011	0.181	0.002	0.165	0.065	0.456	0.026	0.141	0.190	0.007	0.184	0.074	0.318	0.014
1.819	0.003	0.002	0.005	0.005	0.006	0.001	0.002	0.001	0.004	0.001	0.006	0.001	0.003	0.003	0.001	0.005	0.005	0.004	0.001
		0.931	0.932	0.928	0.600	0.008	1.794	0.007	1.723	0.909	0.615	0.016	1.829	1.809	0.011	1.716	0.897	0.728	0.007
		0.891	0.886	0.908					0.023	0.921			0.000			0.020	0.934		
		0.033	0.032	0.026						0.026			0.001				0.018		
0.007	0.001				0.003	0.001	0.007	0.000	0.002		0.003	0.001	0.008	0.008	0.001		0.000	0.005	0.001
3.004	0.003	4.002	4.001	3.991	3.033	0.003	2.991	0.003	3.988	4.006	3.024	0.005	2.995	3.004	0.004	4.010	4.022	3.015	0.003
0.909	0.002	0.932	0.935	0.941	0.592	0.008	0.908	0.001	0.913	0.933	0.610	0.017	0.929	0.905	0.004	0.903	0.924	0.725	0.007
		0.221	0.215	0.207	0.492	0.007			0.153	0.208	0.432	0.026	0.968			0.089	0.132	0.221	0.015
					4.3	0.3					3.1	0.6						2.1	0.4
					48.6	0.7					55.0	2.5						76.3	1.7
					47.1	0.7					41.8	2.6						21.6	1.4

Numbers in parentheses next to the texture are the same as the sample name in Table 1. amph, amphibole; Anal#, analytical point name (expressed as numbers in parentheses next to the mineral name); c, core; Chr, chromite; Chr(d), dumite layer in chromitite; Cr#, Cr/(Cr + Al) atomic ratio; n, number of analyses; ol, olivine; opx, orthopyroxene; inc, inclusion; Mg#, Mg/(Mg + Fe^{total}) atomic ratio except for chromite (Mg/(Mg + Fe²⁺)) atomic ratio; r, rim; STD, standard deviation; Y Fe, Fe³⁺/(Al + Cr + Fe³⁺); Y Al, Al/(Al + Cr + Fe³⁺); Y Cr, Cr/(Al + Cr + Fe³⁺).

Table 3 Trace-element compositions of clinopyroxenes in the southern area

Rock type Anal# (p.p.m.)	Chromitite			Dunite			Harzburgite			Lherzolite			
	55	71	73 [†]	46	56	93	94	99	100 [†]	18	20	23	24 [†]
Li	<1	1.5	1.8	1.0	1.1	2.9	2.5	2.7	2.4	2.5	3.5	4.5	3.4
Sc	74	86	83	88	92	67	78	70	79	67	67	64	63
Ti	512	473	482	1012	1187	1005	1069	1078	1141	1865	1842	1741	1627
V	97	88	92	212	223	201	214	216	224	315	316	305	296
Cr	6627	6382	5939	6685	8036	7559	7190	8548	7939	9146	8610	9026	8126
Rb	<0.1	<0.14	<0.11	<0.05	<0.05	<0.05	<0.05	<0.05	<0.05	<0.06	<0.05	<0.06	<0.06
Sr	27	19	26	4.9	4.9	2.6	2.7	2.9	2.5	1.3	1.1	1.1	1.1
Y	8.9	9.1	9.6	6.8	7.6	7.4	8.0	8.0	8.1	11.5	11.3	10.9	10.3
Zr	4.1	4.5	4.4	3.3	3.8	3.0	3.3	3.5	3.4	1.0	1.0	1.0	1.0
Nb	0.05	0.04	0.03	0.06	0.06	0.05	0.05	0.05	0.05	0.07	0.07	0.05	0.05
Ba	<0.02	<0.01	<0.02	<0.01	<0.01	<0.01	<0.01	<0.01	<0.01	0.01	<0.01	<0.01	<0.01
La	0.34	0.29	0.36	0.03	0.04	0.02	0.02	0.02	0.01	0.02	0.01	0.02	0.01
Ce	1.3	1.3	1.3	0.22	0.23	0.13	0.11	0.13	0.12	0.07	0.07	0.07	0.09
Nd	1.6	1.5	1.6	0.60	0.55	0.42	0.41	0.50	0.44	0.40	0.47	0.42	0.40
Sm	0.79	0.79	0.83	0.36	0.35	0.31	0.34	0.37	0.37	0.49	0.42	0.45	0.36
Eu	0.31	0.30	0.33	0.14	0.15	0.17	0.14	0.17	0.17	0.22	0.20	0.20	0.22
Gd	1.3	1.3	1.3	0.68	0.67	0.77	0.77	0.79	0.78	1.2	1.1	1.1	1.1
Dy	1.7	1.8	1.9	1.1	1.1	1.2	1.4	1.3	1.3	1.9	1.8	2.0	1.9
Er	1.1	0.90	1.0	0.82	0.93	0.82	0.96	0.92	0.90	1.4	1.3	1.3	1.1
Yb	0.89	0.87	0.83	0.94	0.97	0.79	0.88	0.87	0.95	1.35	1.34	1.29	1.33
Lu	0.11	0.14	0.14	0.12	0.13	0.10	0.12	0.13	0.11	0.19	0.17	0.17	0.15
Hf	0.19	0.26	0.21	0.19	0.17	0.22	0.17	0.21	0.22	0.12	0.16	0.13	0.18
Pb	<0.1	<0.1	<0.1	<0.05	<0.05	<0.05	<0.05	<0.05	<0.05	<0.05	<0.05	<0.06	<0.05
(Ce/Yb) _n	0.39	0.39	0.42	0.061	0.061	0.042	0.034	0.040	0.034	0.014	0.014	0.015	0.018

Dunite, harzburgite and lherzolite samples were collected near the chromitite, of which trace-element compositions of clinopyroxene inclusions within chromite were analyzed. [†]Major-element compositions are shown in Table 2.

Anal#, analytical point name; (Ce/Yb)_n, chondrite-normalized Ce/Yb ratio.

TRACE ELEMENT COMPOSITIONS OF CLINOPYROXENE

Chondrite-normalized REE patterns (CH-normalized REE patterns hereafter) of all clinopyroxenes generally show depletion of the LREE (Fig. 3). Lherzolite near the chromitites contains a clinopyroxene with a strongly LREE depleted abundance ($(\text{Ce}/\text{Yb})_n = 0.014\text{--}0.018$). It is interesting to note that the LREE and Sr contents of clinopyroxenes in dunite and chromitite are apparently higher than those of the host peridotites near the chromitites (Table 3). In particular, clinopyroxene inclusions within chromite are apparently higher in LREE (+Sr) contents than others and are depleted in heavy rare earth elements (HREE) ($(\text{Ce}/\text{Yb})_n = 0.39\text{--}0.42$), resulting in a convex CH-normalized REE pattern (Fig. 3). LREE contents in harzburgite near the chromitites also tend to be higher than those in lherzolite, whereas HREE are low ($(\text{Ce}/\text{Yb})_n = 0.034\text{--}0.042$ for harzburgites). High field strength element (Nb, Zr, Hf) and V contents in the clinopyroxene inclusion may be affected by the presence of chromite because these elements are relatively partitioned into the chromite compared with other elements (e.g. REE, which have very low content; Egginis *et al.* 1998). The Rb, Ba and Pb contents are usually lower than the detection limits of the analyses ($<0.5\text{--}0.1$ p.p.m., $<0.01\text{--}0.02$ p.p.m. and $<0.05\text{--}0.10$ p.p.m., respectively). The variations of these elements in clinopyroxenes are not discussed here because of the difficulties and uncertainties in both the analysis and distribution of the elements.

DISCUSSION

ORIGIN OF CHROMITITE IN THE LHERZOLITE-DOMINANT MANTLE SECTION

The presence of massive-type chromitites suggests that only chromite was crystallized for a period of time and/or was concentrated by flow differentiation during the crystallization of chromite grains and/or deformation-induced selective accumulation after crystallization of the chromite grains in the formation of the chromitites. Pyroxene inclusions within the chromites are more abundant in the massive-type and nodular-type chromitites than in other types. It is inconceivable that chromite with pyroxene inclusions was selectively concentrated for the formation of the massive-type and nodular-type chromitites by these physical mechanisms only. Hence, chromites in the massive-type chromitites might have been

simultaneously precipitated with pyroxenes (\pm amphibole) from a melt. LREE and Sr abundances in clinopyroxene inclusions within chromites in the chromitites are the highest among the studied samples. It is concluded that the melts responsible for the formation of chromitites were enriched with Cr, Si and incompatible elements (Na, LREE, Sr and H_2O). Reaction between the host peridotites and primitive basaltic melts of deeper origin results in selective dissolution of pyroxene and, in turn, crystallization of olivine (i.e. formation of the dunite envelopes) to produce a modified melt rich in SiO_2 (e.g. Fisk 1986; Kelemen 1990). During the formation of the massive-type and nodular-type chromitites, decreasing of melt mass as a result of crystallization of chromite, coupled with a zone-refining effect (Harris 1957; Kushiro 1968), would have resulted in effective enrichment of incompatible elements such as LREE, Sr, Na and H_2O in modified melts (Arai *et al.* 1997; Morishita *et al.* 2004). The local concentration of chromite with pyroxene inclusions has therefore been explained by crystallization from a hybridized melt because the hybridized melt moves into the chromite stability field as already proposed for the formation of podiform chromitites in other ophiolites and ocean floors by Arai and Yurimoto (1994), Zhou (1994) and Arai and Matsukage (1998). The hybridized melt was formed by the mixing of primitive basaltic melts with Si-rich secondary melts as a result of the reaction between the primitive basaltic melts and wall peridotites. The dunite envelope of the chromitite would be of replacive origin, which is similar to discordant dunite commonly found in mantle peridotites (Quick 1981; Kelemen 1990).

Thin dunite layers without large chromitite frequently found in the Isabela ophiolite are also thought to be of replacive origin as a result of melt–rock interaction rather than cumulate and/or residue after a high degree of partial melting (Andal *et al.* 2005). This is supported by chromite trails after pyroxenites, where dunites cross-cut the layering of peridotites and pyroxenites. The presence of the replacive dunites in the studied area indicates that melt–rock interactions occurred in the whole area, but did not always lead to the formation of chromitites.

Arai and Abe (1995) and Arai (1997a,b) suggested that a moderately refractory harzburgite, which has chromite with an intermediate Cr# (~ 0.5), is the most suitable host for large-scale podiform chromitites. This is consistent with the field observations, coupled with mineral compositions

between the chromitites and their host peridotites in the present study. In the study area, large chromitites (+dunite envelope) only occur in relatively depleted harzburgite, although the Isabela ophiolite is a lherzolite-dominant ophiolite. The Cr# of chromites in the harzburgite near the chromitites falls into high end to higher than those of the whole range from clinopyroxene-bearing harzburgite to lherzolite far from the chromitites in the Isabela ophiolite (Fig. 2). Such lithological gradation from chromitite to dunite to harzburgite to clinopyroxene-rich harzburgite (almost lherzolite in terms of the Cr# of chromite, ~0.2) was also reported in the Luobusa ophiolites, China (Zhou *et al.* 1996).

The next question is the genetic relationship between the chromitites and the surrounding depleted harzburgites. There are two plausible relationships between them: (i) the depleted harzburgites had previously formed in the mantle section before the chromitites were formed; or (ii) the depleted harzburgites were formed by the same magmatic activity responsible for the formation of the chromitites.

In terms of the relationships between the Fo content of olivine and the Cr# of chromite, the harzburgites and lherzolites near the chromitites are typical residual peridotites after a variable degree of partial melting (Arai 1994a,b). Conversely, the LREE abundance of clinopyroxene in the harzburgites near the chromitites is higher than that in the surrounding lherzolites, although the LREE abundance in clinopyroxenes constantly decreases from lherzolite to harzburgite far from large chromitites (Andal *et al.* 2005; Fig. 3). Furthermore, the TiO₂ content of chromite slightly increases from lherzolite to harzburgite near the chromitites (Fig. 5). These geochemical characteristics indicate that the harzburgites near the chromitites are not a simple residual peridotite after partial melting from the surrounding lherzolites, whereas harzburgites far from the chromitites show geochemical characteristics of simple residue from surrounding lherzolites (Fig. 3). An inverse correlation between the refractoriness of residual peridotites represented by the major element compositions of minerals and LREE abundance (or LREE/HREE ratios) is commonly found in peridotite xenoliths (e.g. Frey & Green 1974) and orogenic peridotites (e.g. Frey *et al.* 1991; Takazawa *et al.* 1992; Ozawa & Shimizu 1995). The inverse correlation can be caused by open-system melting – that is, melting associated with an influx of

LREE-enriched fluids/melts (Ozawa & Shimizu 1995).

It should be emphasized that a small chromitite pod was found only in a relatively thick dunite layer, although there are many thin dunite layers without chromitites in the same area. This means that the formation of chromitites would be restricted in large melt conduits where melt supply is expected to be high and melts were multiply supplied. When the melt supply is high, the ascent of basaltic melts of deep origin would cause partial melting of the fertile lherzolitic wall-rock at low pressure conditions to leave depleted harzburgites (e.g. Takahashi 1992; Fig. 6). When the magma supply is low like a branch of large melt conduits, it might be insufficient to increase the temperature to melt even in the fertile peridotite walls, but can form the replacive dunite as a result of the selective dissolution of orthopyroxenes by melt–rock interactions (Fig. 6). Once the depleted harzburgites were formed in the large melt conduit, the secondary melts enriched with both Cr and Si (+LREE, Sr, Na and H₂O) were formed as a result of interaction with the depleted peridotites and subsequently supplied primitive melts. It is possible that newly supplied primitive melts can mix with the secondary melts within the same large melt conduits to solely precipitate chromite (Fig. 6). Thus, in the present study, the simultaneous formation of the chromitites and the surrounding depleted harzburgites in the Isabela ophiolite is favored.

Implications for the tectonic setting of the Isabela ophiolite

The tectonic setting for the formation of chromitite is still a matter of debate (e.g. Roberts 1988; Arai 1995, 1998; Prichard *et al.* 1996; Robinson *et al.* 1997; Schiano *et al.* 1997; Zhou & Robinson 1997; Zhou *et al.* 1998). Chromitite xenoliths with nodular textures in alkali basalts, derived from the upper mantle of the Southwest Japanese Arc, could support a subarc origin for podiform chromitite (Arai 1978; Arai & Abe 1994). In contrast, a micropod of chromitite, which is lithologically the same as the typical podiform chromitites in ophiolites, was also found in the transition dunite formed at the East Pacific Rise during Leg 147 of the Ocean Drilling Project (ODP; Arai & Matsukage 1998). Hydrous silicate mineral inclusions within chromite are common in chromitite in ophiolites (Talkington *et al.* 1986; Augé 1987; McElduff & Stumpfl 1991; Matsumoto *et al.* 1995; Ahmed *et al.* 2001; Ahmed & Arai 2002), and have also

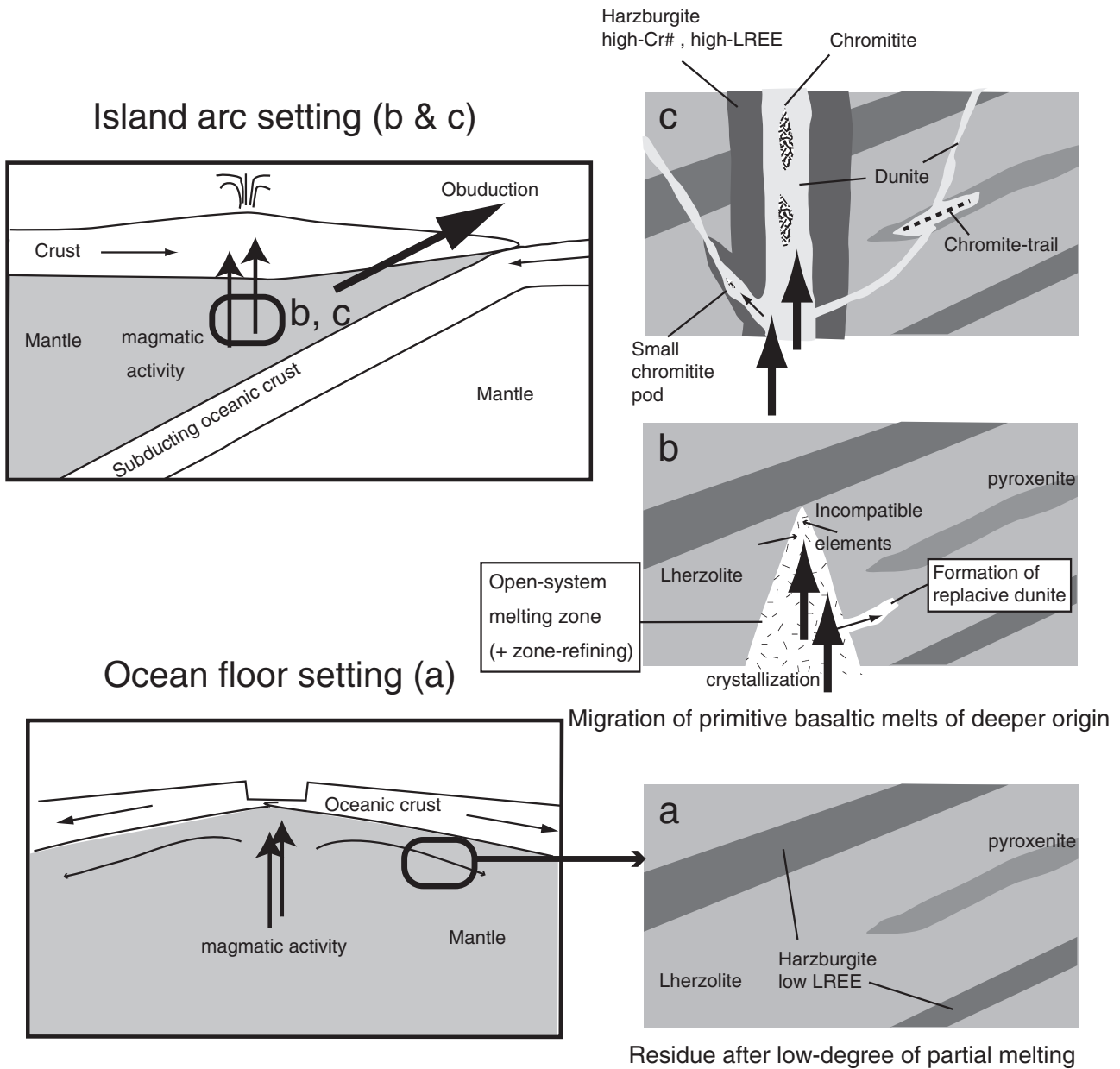


Fig. 6 Schematic cross-section illustrating the formation of the chromitites in a lherzolite-dominant mantle section of the Isabela ophiolite. (a) Layering of lherzolite and clinopyroxene-bearing harzburgite (\pm pyroxenites) already formed by magmatism and deformation beneath the ocean floor before the formation of the chromitites. (b) Beginning stage of migration of primitive melts of deeper origin. In a large melt conduit where melt supply is high, open-system melting was caused by the influx of the primitive melts to leave depleted harzburgite with high light rare earth element (LREE) abundances. In a small conduit where melt supply is low, chromitite-free dunite layers were formed by melt–rock interactions. (c) In the large melt conduit, the secondary melt enriched with both Cr and Si (+LREE, Sr, Na and H₂O) was formed as a result of the interaction with depleted harzburgite and subsequently supplied primitive melts. Chromitites are formed from hybridized melts formed by mixing of the secondary melts and primitive melts within the same melt conduit.

been found in a chromitite micropod collected from the ocean floor (the East Pacific Rise in ODP Leg 147) (Arai & Matsukage 1998; Matsukage & Arai 1998). This means that the hydrous mineral inclusions within chromite can be formed even in almost anhydrous conditions, such as beneath a mid-ocean ridge, and there is therefore no direct evidence for the formation of chromitites under hydrous condi-

tions, such as in a supra-subduction setting (Arai 1998). These observations imply that the podiform chromitite (\pm hydrous silicate mineral inclusions) can be produced in either oceanic or arc-related settings (Arai 1997a,b).

As suggested above, the Isabela ophiolite may be of a slow-spreading ridge origin (Andal *et al.* 2005). The chemical composition of chromite is a

good indicator for the tectonic setting of chromitite formation (Arai 1997a,b). Chromitite with Cr# higher than 0.7 has never been reported in either primitive volcanics or peridotites collected from the ocean floor (Cr# \leq 0.6) (Dick & Bullen 1984; Dick 1989; Arai 1992, 1994a,b; Arai & Matsukage 1998). Cross-cutting dunite layers, including the dunite envelopes of the podiform chromitites, indicate younger generation than the formation of mineral foliation in peridotites. The relatively high-Cr# chromitite (Cr# \geq 0.65) in podiform chromitites may indicate a genetic link with arc-related magmas, such as high-Mg andesite and boninites (Arai & Yurimoto 1994; Robinson *et al.* 1997). It is concluded that the upper mantle section of the Isabela ophiolite was initially formed at the ocean floor in a slow-spreading mid-ocean ridge setting, and was followed by a magmatism related to a supra-subduction setting in response to a switch of tectonic setting as a consequence of the origin of ophiolite, which is an obducted oceanic lithosphere at plate convergent margins. A similar tectonic switch has been already reported in the mantle section of the Luobusa ophiolite, China (Zhou *et al.* 1996), the Zambales ophiolite complex, the Philippines (Yumul 1992), and the Oman ophiolite (Ahmed & Arai 2002), where younger high-Cr chromitites were formed in old mid-oceanic ridge basalt-type peridotites.

CONCLUSIONS

The petrology and geochemical characteristics of chromitites and their host peridotites in the Isabela ophiolite are summarized below:

1. Chromitites show podiform, nodular, layered and disseminated textures and are typical podiform chromitites. They occur in harzburgite hosts characterized by relatively high-Cr# and high-LREE contents as compared with clinopyroxene-bearing harzburgites far from the chromitites (Fig. 3).
2. Silicate mineral inclusions (olivine, clinopyroxene, amphibole and orthopyroxene) of chromite are frequently found in the chromitites. Pyroxene (\pm amphibole) inclusions are more abundant in the massive-type chromitites than in others.
3. Clinopyroxene inclusions of chromite in the chromitites show high LREE and low HREE compared with clinopyroxenes in the host peridotites. The chromitites were precipitated from melts enriched with Cr, Si and incompatible elements (LREE, Sr, Na, H₂O), which were formed by melt–rock interactions coupled with a zone-refining effect.
4. The relatively depleted harzburgite hosts near the chromitites were simultaneously formed with the chromitites in large melt conduits where the melt supply is expected to be high. The harzburgite host was formed by partial melting coupled with the influx of primitive basaltic melts of deeper origin. The chromitites were precipitated with silicate inclusions from hybridized melts formed by the mixing of SiO₂-rich secondary melts after melt–rock interaction and the primitive melts continuously supplied to the melt conduit.
5. The Cr# of chromite in the chromitites is 0.65–0.75, which is compatible with the range for arc-related magmas, although that of the peridotites is compatible with the range for mid-ocean ridge magmas (Fig. 2). The mantle section of the Isabela ophiolite was initially formed beneath a slow-spreading mid-ocean ridge followed by arc-related magma (Fig. 6). The chromitite was formed at arc stages.

ACKNOWLEDGEMENTS

We wish to acknowledge the support of the 21st Century COE project (led by K. Hayakawa) and the Incubation Business Laboratory Center of Kanazawa University. Kazue Tazaki, Jiro Uesugi, Yohei Shimizu, Satoko Ishimaru, Miki Shirasaka and Akihiro Tamura-Hasebe are thanked for EPMA and LA-ICP analyses. Constructive reviews by Françoise Boudier and Piera Spadea and comments from Akira Ishiwatari much improved the manuscript.

REFERENCES

- AHMED A. H. & ARAI S. 2002. Unexpectedly high-PGE chromitite from the deeper mantle section of the northern Oman ophiolite and its tectonic implications. *Contributions to Mineralogy and Petrology* **143**, 263–78.
- AHMED A. H., ARAI S. & ATTIA A. K. 2001. Petrological characteristics of podiform chromitites and associated peridotites of the Pan African Proterozoic ophiolite complexes of Egypt. *Mineralium Deposita* **36**, 72–84.
- ANDAL E. S., ARAI S. & YUMUL G. P. JR 2005. Complete mantle section of a slow spreading ridge-derived ophiolite: An example from the Isabela Ophiolite (Philippines). *Island Arc* **14**, 272–94.

- ARAI S. 1978. A massive chromitite nodule in alkali olivine basalt from Takashima, Southwestern Japan. *Report of Faculty of Science, Shizuoka University* **12**, 99–113.
- ARAI S. 1992. Chemistry of chromian spinel in volcanic rocks as a potential guide to magma chemistry. *Mineralogical Magazine* **56**, 173–84.
- ARAI S. 1994a. Characterization of spinel peridotites by olivine–spinel compositional relationships: Review and interpretation. *Chemical Geology* **113**, 191–204.
- ARAI S. 1994b. Compositional variation of olivine–chromian spinel in Mg-rich magmas as a guide to their residual spinel peridotites. *Journal of Volcanology and Geothermal Research* **59**, 279–93.
- ARAI S. 1995. Possible sub-arc origin of podiform chromitites. *Island Arc* **4**, 104–11.
- ARAI S. 1997a. Control of wall-rock composition on the formation of podiform chromitites as a result of magma/peridotite interaction. *Resource Geology* **47**, 177–87.
- ARAI S. 1997b. Origin of podiform chromitites. *Journal of Asian Earth Sciences* **15**, 303–10.
- ARAI S. 1998. Comments of the paper 'Primitive basaltic melts included in podiform chromites from the Oman ophiolite' by P. Schiano *et al.* *Earth and Planetary Science Letters* **156**, 117–19.
- ARAI S. & ABE N. 1994. Podiform chromitite in the arc mantle: Chromitite xenoliths from the Takashima alkali basalt, Southwest Japan arc. *Mineralium Deposita* **29**, 434–8.
- ARAI S. & ABE N. 1995. Reaction of orthopyroxene in peridotite xenoliths with alkali-basalt melt and its implication for genesis of alpine-type chromitite. *American Mineralogist* **80**, 1041–7.
- ARAI S. & MATSUKAGE K. 1998. Petrology of a chromitite micropod from Hess Deep, equatorial Pacific: A comparison between abyssal and alpine-type podiform chromitites. *Lithos* **43**, 1–14.
- ARAI S., MATSUKAGE K., ISOBE E. & VYSOTSKIY S. 1997. Concentration of incompatible elements in oceanic mantle: Effect of melt/wall interaction in stagnant or failed melt conduits within peridotite. *Geochimica et Cosmochimica Acta* **61**, 671–5.
- ARAI S. & YURIMOTO H. 1994. Podiform chromitites of the Tari-Misaka ultramafic complex, southwestern Japan, as mantle–melt interaction products. *Economic Geology* **89**, 1279–88.
- AUGÉ T. 1987. Chromite deposits in the northern Oman ophiolite: Mineralogical constraints. *Mineralium Deposita* **22**, 1–10.
- BILLEDÓ E., STEPHAN J. F., DELTEIL J., BELLON H., SAJONA F. & FERAUD G. 1996. The pre-Tertiary ophiolitic complex of northeastern Luzon and the Polillo group of islands, Philippines. *Journal of the Geological Society of the Philippines* **LI**, 95–114.
- BOUDIER F. & NICOLAS A. 1985. Harzburgite and lherzolite subtypes in ophiolitic and oceanic environments. *Earth and Planetary Science Letters* **76**, 84–92.
- CASSARD D., NICOLAS A., RABINOVITCH M., MOUTTE J., LEBLANC M. & PRINZHOFER A. 1981. Structural classification of chromite pods in southern New Caledonia. *Economic Geology* **76**, 805–31.
- DICK J. B. H. 1989. Abyssal peridotites, very slow spreading ridges and ocean ridge magmatism. In Saunders A. D. & Norry M. J. (eds). *Magmatism of Ocean Basins. Geological Society Special Publication* **42**, 71–105.
- DICK J. B. H. & BULLEN T. 1984. Chromian spinel as a petrogenetic indicator in abyssal and alpine-type peridotites and spatially associated lavas. *Contributions to Mineralogy and Petrology* **86**, 54–76.
- DIMALANTA C. B. & YUMUL G. P. JR 2004. Crustal thickening in an active margin setting (Philippines): The whys and the hows. *Episode* **27**, 260–64.
- EGGINS S. M., RUDNICK R. L. & MCDONOUGH W. F. 1998. The composition of peridotites and their minerals: A laser-ablation ICP-MS study. *Earth and Planetary Science Letters* **154**, 53–71.
- FISK M. R. 1986. Basalt magma interaction with harzburgite and the formation of high-magnesium andesites. *Geophysical Research Letters* **13**, 467–70.
- FREY F. A. & GREEN D. H. 1974. The mineralogy, geochemistry and origin of lherzolite inclusions in Victorian basanites. *Geochimica et Cosmochimica Acta* **38**, 1023–59.
- FREY F. A., SHIMIZU N., LEINBACH A., OBATA M. & TAKAZAWA E. 1991. Compositional variations within the lower layered zone of the Horoman peridotite, Hokkaido, Japan: Constraints on models for melt–solid segregation. *Journal of Petrology*, Special Lherzolite Issue, 211–27.
- GERVILLA F. & LEBLANC M. 1990. Magmatic ores in high-temperature alpine-type lherzolite massifs (Ronda, Spain, and Beni Bousera, Morocco). *Economic Geology* **85**, 112–32.
- HARRIS P. G. 1957. Zone refining and the origin of potassic basalts. *Geochimica et Cosmochimica Acta* **12**, 195–208.
- IRVINE T. N. 1965. Chromian spinel as a petrogenetic indicator. Part 1, theory. *Canadian Journal of Earth Sciences* **2**, 648–72.
- IRVINE T. N. 1967. Chromian spinel as a petrogenetic indicator. Part 2, petrologic applications. *Canadian Journal of Earth Sciences* **4**, 71–103.
- IRVINE T. N. 1975. Crystallization sequences in the Muskox intrusion and other layered intrusions – II. Origin of chromitite layers and similar deposits of other magmatic ores. *Geochimica et Cosmochimica Acta* **39**, 991–1020.
- IRVINE T. N. 1977. Origin of chromitite layers in the Muskox intrusion and other stratiform intrusions: A new interpretation. *Geology* **5**, 273–7.
- ISHIDA Y., MORISHITA T., ARAI S. & SHIRASAKA M. 2004. Simultaneous in-situ multi-element analysis of

- minerals on thin section using LA-ICP-MS. *Science Reports of Kanazawa University* **48**, 31–42.
- JACKSON E. D. 1969. Chemical variation in coexisting chromite and olivine in chromitite zone of the Stillwater complex. In Wilson H. D. B. (ed.). *Magmatic Ore Deposit. Economic Geology Monograph* **4**, 41–71.
- JOHNSON K. T. M. & DICK H. J. B. 1992. Open system melting and temporal and spatial variation of peridotite and basalt at the Atlantis II Fracture Zone. *Journal of Geophysical Research* **97**, 9219–41.
- KELEMEN P. B. 1990. Reaction between ultramafic rocks and fractionating basaltic magma I. Phase relations, the origin of calc-alkaline magma series, and the formation of discordant dunite. *Journal of Petrology* **31**, 51–98.
- KUSHIRO I. 1968. Compositions of magmas formed by partial zone melting in the earth's upper mantle. *Journal of Geophysical Research* **73**, 619–34.
- LEAKE B. E., WOOLLEY A. R., ARPS C. E. S. *et al.* 1997. Nomenclature of amphiboles: Report of the subcommittee on amphiboles of the International Mineralogical Association, Commission on New Minerals and Mineral Names. *American Mineralogist* **82**, 1019–37.
- LEBLANC M. & TEMAGOULT A. 1989. Chromite pods in a lherzolite massif (Collo, Algeria): Evidence of oceanic-type mantle rocks along the West Mediterranean Alpine Belt. *Lithos* **23**, 153–62.
- LONGERICH H. P., JACKSON S. E. & GÜTHER D. 1996. Laser ablation inductively coupled plasma mass spectrometric transient signal data acquisition and analyte concentration calculation. *Journal of Analytical Atomic Spectrometry* **11**, 899–904.
- LORAND J. P. & CEULENEER G. 1989. Silicate and base-metal sulfide inclusions in chromitites from the Maqsad area (Oman ophiolite, Gulf of Oman): A model for entrapment. *Lithos* **22**, 173–90.
- MCDONOUGH W. F. & SUN S.-S. 1995. The composition of the Earth. *Chemical Geology* **120**, 223–53.
- MCELDUFF B. & STUMPFL E. F. 1991. The chromite deposits of the Troodos Complex, Cyprus – evidence for the role of a fluid phase accompanying chromite formation. *Mineralium Deposita* **26**, 307–18.
- MATSUKAGE K. & ARAI S. 1998. Jadeite, albite and nepheline as inclusions in spinel of chromitite from Hess Deep, equatorial Pacific: Their genesis and implications for serpentinite diapir formation. *Contributions to Mineralogy and Petrology* **131**, 111–22.
- MATSUMOTO I., ARAI S. & HARADA T. 1995. Hydrous mineral inclusions in chromian spinel from the Yanaomine ultramafic complex of the Sangun zone, Southwest Japan. *Journal of Mineralogy, Petrology and Economic Geology* **90**, 333–8 (in Japanese with English abstract).
- MORISHITA T., ISHIDA Y. & ARAI S. 2005a. Simultaneous determination of multiple trace element compositions in thin (<30 µm) layers of BCR-2G by 193 nm ArF excimer laser ablation-ICP-MS: Implications for matrix effect and element fractionation on quantitative analysis. *Geochemical Journal* **39**, 327–40.
- MORISHITA T., ISHIDA Y., ARAI S. & SHIRASAKA M. 2005b. Determination of multiple trace element compositions in thin (<30 µm) layers of NIST SRM 614 and 616 using laser ablation ICP-MS. *Geostandards and Geoanalytical Research* **29**, 107–22.
- MORISHITA T., MAEDA J., MIYASHITA S., MATSUMOTO T. & DICK H. J. 2004. Magmatic srilankite (Ti₂ZrO₆) in gabbroic vein cutting oceanic peridotites: An unusual product of peridotite–melt interactions beneath slow-spreading ridges. *American Mineralogist* **89**, 759–66.
- NICOLAS A. 1989. *Structure of Ophiolite and Dynamics of Oceanic Lithosphere*. Kluwer, Dordrecht.
- NICOLAS A. & AL AZRI H. 1991. Chromite-rich and chromite-poor ophiolites: The Oman Case. In Peters T. J., Nicolas A. & Coleman R. G. (eds). *Ophiolite Genesis and Evolution of the Oceanic Lithosphere*, pp. 261–74. Kluwer, Dordrecht.
- NOLLER J. S. & CARTER B. 1986. The origin of various types of chromite schlieren in the Trinity Peridotite, Klamath Mountains, California. In Carter B., Chowdhury M. K. R. & Jankovic, S. (eds). *Metallogeny of Basic and Ultrabasic Rocks (Regional Presentations)*, pp. 151–78. Theophrastus, Athens.
- OZAWA K. 1983. Evaluation of olivine-spinel geothermometry as an indicator of thermal history for peridotites. *Contributions to Mineralogy and Petrology* **82**, 52–65.
- OZAWA K. & SHIMIZU N. 1995. Open-system melting in the upper mantle: Constraints from the Hayachine-Miyamori ophiolite, northeastern Japan. *Journal of Geophysical Research* **100**, 22 315–35.
- PEARCE N. J. G., PERKINS W. T. & WESTGATE J. A. *et al.* 1997. A compilation of new and published major and trace element data for NIST SRM 610 and NIST SRM 612 glass reference materials. *Geostandards Newsletter: The Journal of Geostandards and Geoanalysis* **21**, 114–44.
- PRICHARD H. M., LORD R. A. & NEARY C. R. 1996. A model to explain the occurrence of platinum- and palladium-rich ophiolite complexes. *Journal of the Geological Society, London* **153**, 323–8.
- QUICK J. E. 1981. The origin and significance of large, tabular dunite bodies in the Trinity Peridotite, northern California. *Contributions to Mineralogy and Petrology* **78**, 413–22.
- ROACH T. A., ROEDER P. L. & HULBERT L. J. 1998. Composition of chromite in the upper chromitite, Muskox layered intrusion, Northwest Territories. *Canadian Mineralogist* **36**, 117–35.
- ROBERTS S. 1988. Ophiolitic chromitite formation: A marginal basin phenomenon? *Economic Geology* **83**, 1034–6.

- ROBINSON P. T., ZHOU M. F., MALPAS J. & BAI W.-J. 1997. Podiform chromitites: Their composition, origin and environment of formation. *Episodes* **20**, 247–52.
- SCHIANO P., CLOCCHIATTI R., LORAND J.-P., MASSARE D., DELOULE E. & CHAUSSIDON M. 1997. Primitive basaltic melts included in podiform chromites from the Oman Ophiolite. *Earth and Planetary Science Letters* **146**, 489–97.
- TAKAHASHI N. 1992. Evidence for melt segregation towards fractures in the Horoman mantle peridotite complex. *Nature* **359**, 52–5.
- TAKAZAWA E., FREY F. A., SHIMIZU N. & OBATA M. 1992. Geochemical evidence for melt migration and reaction in the upper mantle. *Nature* **359**, 55–8.
- TALKINGTON R. W., WATKINSON D. H., WHITTAKER P. J. & JONES P. C. 1986. Platinum group element-bearing minerals and other solid inclusions in chromite of mafic and ultramafic complexes: Chemical compositions and comparisons. In Carter B., Chowdhury M. K. R. & Jankovic S. (eds). *Metallogeny of Basic and Ultrabasic Rocks (Regional Presentations)*, pp. 223–49. Theophrastus, Athens.
- THAYER T. P. 1964. Principal features and origin of podiform chromite deposits, and some observations on the Guleman-Soridag district, Turkey. *Economic Geology* **59**, 1497–524.
- YUMUL G. P. JR 1992. Ophiolite-hosted chromitite deposits as tectonic setting and melting degree indicators: Examples from the Zambales Ophiolite Complex, Luzon, Philippines. *Mining Geology* **42**, 5–17.
- YUMUL G. P. JR, BALCE G. R., DIMALANTA C. B. & DATUIN R. T. 1997. Distribution, geochemistry and mineralization potentials of the Philippine ophiolite and ophiolitic sequences. *Ophioliti* **22**, 47–56.
- ZHOU M.-F. 1994. Formation of podiform chromitites by melt/rock interaction in the upper mantle. *Mineralium Deposita* **29**, 98–101.
- ZHOU M.-F. & ROBINSON P. 1997. Origin and tectonic environment of podiform chromite deposits. *Economic Geology* **92**, 259–62.
- ZHOU M.-F., ROBINSON P., MALPAS J. & LI Z. 1996. Podiform chromitites in the Lubusa ophiolite (southern Tibet): Implications for melt–rock interaction and chromite segregation in the upper mantle. *Journal of Petrology* **37**, 3–21.
- ZHOU M.-F., SUN M., KEAYS R. R. & KERRICH R. W. 1998. Controls on platinum-group elemental distributions of podiform chromitites: A case study of high-Cr and high-Al chromitites from Chinese orogenic belts. *Geochimica et Cosmochimica Acta* **62**, 677–88.